Rapid laser reactive sintering of $BaCe_{0.7}Zr_{0.1}Y_{0.1}Yb_{0.1}O_{3-\delta}$ electrolyte for protonic ceramic fuel cells

Shenglong Mu [a,1], Hua Huang [a,1], Akihiro Ishii [a], Zeyu Zhao [a], Minda Zou [a], Patrick Kuzbary [a], Fei Peng [a], Kyle S. Brinkman [a], Hai Xiao [b], Jianhua Tong [a,*]

[a] Materials Science and Engineering, Clemson University, Clemson, SC29634, USA
[b] Electrical and Computer Engineering, Clemson University, Clemson, SC29634, USA

ABSTRACT

The state-of-the-art protonic ceramic electrolyte $BaCe_{0.7}Zr_{0.1}Y_{0.1}Yb_{0.1}O_{3-\delta}$ (BCZYYb) dense films were successfully deposited on the pre-sintered Ni(O)+BCZYYb anode substrate by recently developed rapid laser reactive sintering (RLRS) method. The separation of the deposition of dense electrolyte from the preparation of porous anode makes it possible to manufacture protonic ceramic fuel cells (PCFCs) with more desirable electrolyte and anode microstructures. The PCFC single cells prepared after introducing the cathode thin film $BaCo_{0.4}Fe_{0.4}Zr_{0.1}Y_{0.1}O_{3-\delta}$ (BCFZY0.1) showed OCVs of 0.94–0.97V and peak power densities of 97 mW/cm^2 at 600 °C and 121 mW/cm^2 at 600–650 °C under Air/H_2 gradient. The proton conductivity of the BCZYYb film derived the RLRS-derived single cell showed a moderate proton conductivity of 3.7×10^{-3} S/cm at 600 °C. The higher PCFC performance can be expected by further optimization of the thickness, compositions, and/or microstructures of the component layers.

1. Introduction

Protonic ceramics show high ionic conductivities at intermediate temperatures (300–600 °C) because of their low activation energy for proton transportation [1]. This unique property makes them promising electrolytes for solid oxide electrochemical devices such as protonic ceramic fuel cells (PCFCs) [2], electrolysis cells [3], reversible PCFCs [4–7], and membrane reactors [8,9]. However, to prepare the fully densified protonic ceramic electrolyte membranes having a high proton conductivity, the sintering at high temperature (1600–1700 °C) for a long time (>10h) is generally required since the state-of-the-art protonic ceramics of the acceptor-doped barium zirconate–cerate is very refractory [10,11]. This long-term and the high-temperature sintering usually is a problematic process, especially for the commonly used co-firing method, which has extensively used for the fabrication of solid oxide fuel cells, including PCFCs [3,12–15]. As shown in Fig. S1a, to achieve a fully densified electrolyte thin membrane, the dual green layers of electrolyte and anode have to be sintered at high temperature (1400–1600 °C for a long time (>10h), which makes it impossible to get a well-controlled nanoporous microstructure for high-performance anodes. The challenge is going to be more severe when operating the fuel

cells with non-hydrogen fuels (e.g., hydrocarbons). Recently, several creative techniques for lowering the sintering temperature and shorting the sintering time have been reported [16–22] Among them, the solid state reactive sintering (SSRS) method could lower the sintering temperature to ~1400 °C. However, the sintering time longer than 10 h was still required to ensure the desired crystal and microstructure of electrolytes. Therefore, although the conflict between the requirement for the nanoporous anode and the fully densified electrolyte was mitigated a little bit due to the decrease in sintering temperature, the temperature of 1400 °C is still very high to achieve nanoporous anode.

It is out of the question that the best way to achieve nanoporous anode and fully densified electrolyte is to fire the two layers separately. The physical vapor deposition [23,24] and chemical vapor deposition have been used to deposit the dense electrolyte layers on the pre-sintered anode substrates [25,26]. However, the complicated procedures, expensive equipments, and limitation to sample size made them impractical for large-scale fabrication of PCFCs. Most recently, we developed rapid laser reactive sintering (RLRS) for the advanced manufacturing of protonic ceramic [1,27–31]. The rapid scanning of the high-energy CO_2 laser beam allowed the rapid manufacturing of protonic ceramic with the desired crystal structure and microstructure. The RLRS

has been proved to be much faster and more cost-effective than the SSRS method. The ceramic densification rate is comparable to the ultrafast sintering of ceramic reported by Wang et al. [32]. In this work, as described in Fig. S1b, we fulfilled the fabrication of PCFC single cells in three separate steps for providing the freedom to control the microstructure of each component layer independently. The RLRS showed many advantageous characteristics such as quick and easy to operate, no need for complicated procedures, less energy consumption, and controllable microstructure. The anode pellets of 40 wt%BCZYYb+60 wt%NiO (Ni(O)+BCZYYb) were prepared first by the conventional SSRS method and reduced in the hydrogen atmosphere. Then the dense BCZYYb electrolyte layer was deposited on the top of the as-prepared anode substrate by RLRS. After introducing BCFZY0.1 cathode thin film, the PCFC single cells were obtained, which were characterized for both electrochemical and physical properties.

2. Experiments

The fabrication of PCFC single cells was performed according to the procedure described in Fig. S1b. The primary process of the RLRS electrolyte deposition can be illustrated as follow: (1) preparation of anode substrate; (2) coating of electrolyte precursor thin film; (3) deposition of the dense electrolyte by the RLRS method to form half-cell; (4) the deposition of porous cathode layer to form single cells. The anode pellet substrates consisted of Ni(O)+BCZYYb were prepared using the SSRS method [21]. The stoichiometric amounts of $BaCO_3$, CeO_2, ZrO_2, Y_2O_3, Yb_2O_3, NiO, and 30 wt% starch (pore former) were ball-milled for 48 h using 3 mm YSZ grinding media in isopropanol. The ball-milled powder was pelletized into green pellets with a 1-inch diameter and 5 mm thickness. The green pellets were then fired in the furnace at 1450 °C for 18h, followed by reduced in 5%H_2+95%Ar at 650 °C for 20h.

A green BCZYYb thin layer was cast on the reduced porous Ni(O)+BCZYY anode substrate by a doctor blade. The green BCZYYb paste for casting BCZYYb green films was prepared using the procedure described elsewhere [27,28]. The BCZYYb+1 wt%NiO precursors of $BaCO_3$, CeO_2, ZrO_2, Y_2O_3, Yb_2O_3, and NiO with stoichiometric amounts were mixed by the ball-milling process. The ball-milled BCZYYb+1 wt%NiO electrolyte precursor powder was mixed with de-ionized water, dispersant (DARVAN), and binder (HPMC) to the printable paste. Ther doctor-blade casting was conducted at a 200 μm gap between the frame and the blade, resulted in approximately 150 μm thick after drying at room temperature in the open air for 24 h. The prefired anode substrates were reduced before the laser treatment is aiming to generate more pores in the substrate and reduce the NiO to Ni. The porous structure can avoid the cracking issue of the anode pellets during the laser treatment, as the porous structure can provide anti-crack ability [33–37]. While the Ni in the substrate can conduct the heat faster to avoid the thermal stress generated by the huge temperature gradient [38–40].

The RLRS experiment was performed using a CO_2 laser (λ = 10.6 μm, Ti100W, Synrad). The samples were preheated to 500 °C on a hot plate heated at 500 °C to mitigate thermal shock. The laser beam was focused not by general spherical lenses but by a cylindrical lens (focal length 1 inch, diameter 19.05 mm, Laser Mechanisms, Inc.) to increase the sintering area. The laser parameters of defocus distance, laser energy, and scan speed were set to be 20 mm, 95W, and 0.1 mm/s, respectively, which resulted in a laser beam width of approximately 8 mm for scanning of the samples.

The BCFZY0.1 cathode powder was synthesized by a modified Pechini method as described elsewhere [10]. The detailed procedures for preparing the BCFZY0.1 was shown in the supplementary materials. The as-prepared BCFZY0.1 powder was mixed with the binder (Heraeus V006), and dispersant (solsperse 28000 (Lubrizol)) prepared into paste. The cathode paste was brush painted onto the obtained half-cell and then fired in the air by furnace at 900 °C for 2 h. The PCFC single cells BCFZY0.1 | BCZYYb+1 wt%NiO | Ni(O)–BCZYYb were prepared by depositing BCFZY0.1 cathode thin film on the half cells fabricated by the

RLRS by the conventional screening printing followed by 900 °C furnace treatment for 2 h. A silver paste (T18F014) was used as a current collector. A ceramic bond (552–1219) was used to mount and seal the single cell on an alumina tube. The active area of the single-cell was approximately 0.18 cm^2. The PCFC single cell was first heated to 100 °C at a rate of 1 °C/min and held for 1 h, then heated to 300 °C at the same ramp rate and held for another 1 h to cure the sealant. After that, the cell was increased to 600 at a ramp rate of1.5 °C/min. Both the anode and cathode were exposed in stagnant air during the heating process. 5% H_2 (balance with Ar) with 20 ml/min was fed into anode for the first 6 h, then switched to pure hydrogen for cell testing. Air was swept in the cathode with 150 ml/min. Its I–V characteristic and electrochemical impedance spectra were corrected using a potentiostat (Gamry Reference 3000) at different temperatures. The impedance frequency was ranged from 0.05 to 106 Hz with an amplitude of 10 mV. The temperature rate was controlled at 2 °C/min in this process.

The crystal structure of the samples was characterized using X-ray diffraction (XRD). A Rigaku Ultima IV diffractometer with monochromatic Cu-Kα radiation was used. The XRD pattern was recorded at a rate of 1°/min in the range of 15–85°. The microstructure of the fabricated cells was observed by a scanning electron microscope (SEM Hitachi 4800).

3. Results and discussion

The XRD pattern of the RLRS-derived BCZYYb+1 wt%NiO electrolyte (Fig. 1) shows that the phase-pure perovskite crystal structure was formed, which is the same as the one obtained by the SSRS method. By comparing the XRD patterns (Fig. 1) for Ni(O)-BCZYYb anode substrates after and before the RLRS operation, it can be found that the RLRS did not cause a significant phase composition change in the anode composites, which are still comprised of BCZYYb, NiO, and Ni phases. However, the deeper observation indicated that the amount of NiO increased in the anode composite after the RLRS operation, which, however, did not affect the final performance of PCFC single cells since the NiO was reduced in-situ when operating the fuel cells. The formation of NiO in the anode composite could explain the excellent bonding (will be shown in Fig. 2) between the electrolyte and the anode layer. Therefore, we can conclude that after the RLRS deposition of BCZYYb+1 wt%NiO electrolyte on the reduced Ni(O)+BCZYYb anode substrate, the desired crystal structures for electrolyte and anode were either achieved or kept successfully. However, the reoxidation of Ni to NiO might result in an effect
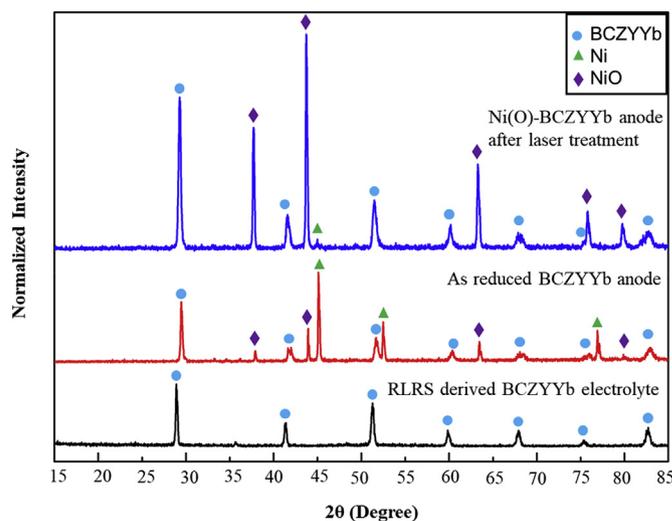

Fig. 1. XRD patterns of RLRS-derived BCZYYb+1 wt%NiO electrolyte and the Ni(O)-BCZYYb anode substrates before (furnace-sintered) and after RLRS operation.
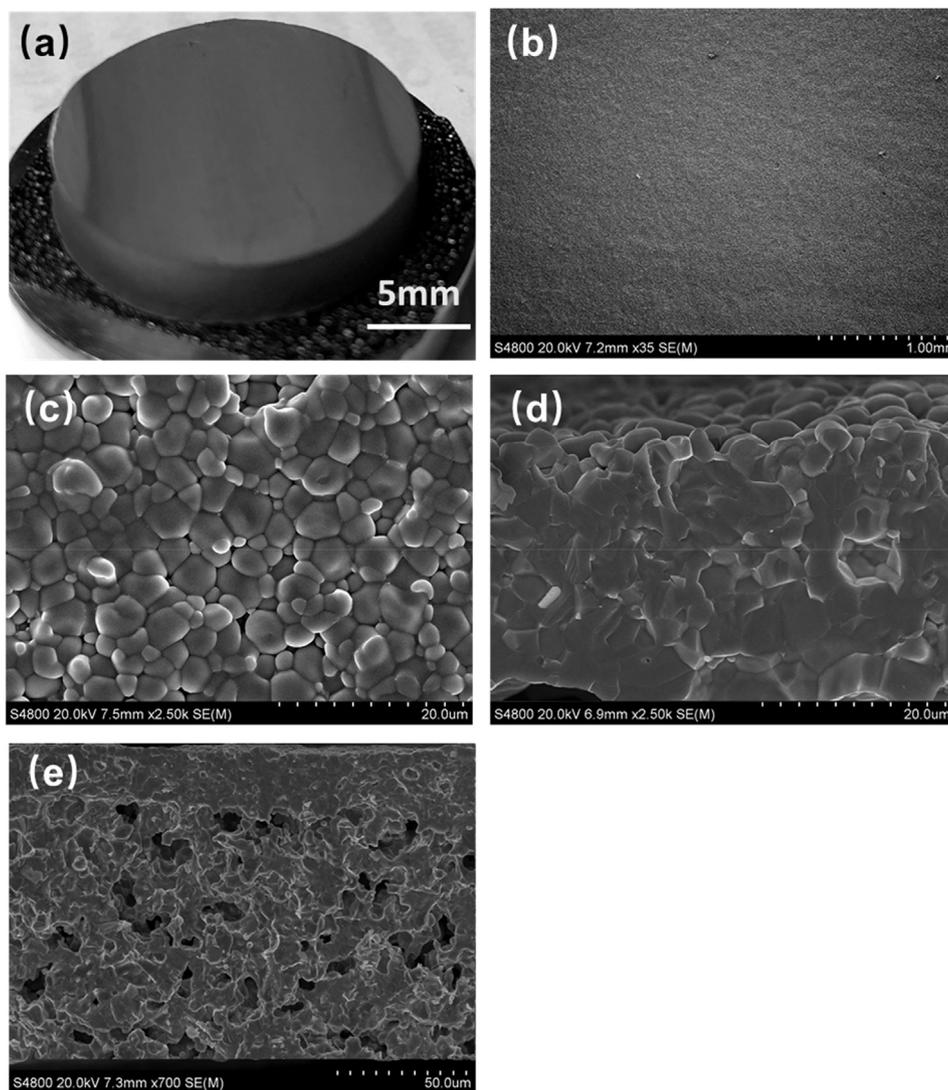
Fig. 2. (a) Photograph of RLRS-derived BCZYYb electrolyte on the Ni(O)–BCZYYb substrate; (b) Low magnification surface SEM micrograph of RLRS-derived BCZYYb electrolyte (c) High magnification surface SEM micrograph of RLRS-derived BCZYYb. (d) High magnification cross-sectional SEM micrograph of RLRS-derived BCZYYb electrolyte; (e) Cross-sectional SEM micrograph of RLRS-derived BCZYYb electrolyte on the Ni(O)–BCZYYb substrate.

on the durability of the PCFCs. We are currently trying to quantify the amount of Ni reoxidation and figure out its effect on the PCFC's performance and stability. We hope to be able to report the Ni reoxidation soon. Indeed, the deposition of cathode might result in Ni reoxidation too, which is also under our current study now.

The photograph (Fig. 2a) of the RLRS-derived BCZYYb+1 wt%NiO electrolyte on the Ni(O)–BCZYYb substrate shows that no visible macrocracks can be observed on the surface of electrolyte layer supported on Ni(O)-BCZYYb anode substrate. The low-magnification SEM micrograph (Fig. 2b) of the electrolyte further shows no microcracks can be observed. The high-magnification SEM micrograph (Fig. 2c) of the electrolyte surface indicates that the electrolyte film is completely defect-free and was fully densified. This grain size (2–5 μm) is comparable to that prepared by the SSRS operation in a furnace [1]. The SEM micrograph (Fig. 2d) of the cross-section of RLRS-derived BCZYYb+1 wt%NiO electrolyte further confirmed that the RLRS-derived electrolyte was fully densified and the grain boundary distance was decreased significantly. The SEM micrograph (Fig. 2e) of the cross-section of half cells with electrolyte supported on anode substrate shows that the anode is still porous after the RLRS operation, which can ensure enough porosity after a further in-situ reduction during fuel cell operation. It can also be clearly seen that the bonding between the electrolyte and anode layer is

excellent. No discontinuity was found at the interface between anode and electrolyte. We can conclude that after the RLRS deposition of BCZYYb+1 wt%NiO electrolyte on Ni(O)-BCZYYb anode substrate, the desired dense microstructure electrolyte was obtained and the desired the porous anode microstructure was kept. The RLRS mechanism for achieving crack-free fully densified electrolyte on pre-sintered anode substrate is still under investigation. The best assumption here is that the RLRS sintering involved the liquid phase sintering like what we have observed during the study of SSRS mechanism [20]. The liquid phase sisntering is supposed to be able remove the stress and allow the only Z-direction shrinkage. In addition, the RLRS method is still relatively new, in which the sintering temperature still cannot easily and accurately measured. The accurate temperature measurement during the RLRS is still under development.

After deposition of BCFZY0.1 cathode thin film, the RLRS-derived half cells were made into BCFZY0.1|RLRS-BCZYYb|Ni(O)-BCZYYb single cells, which was measured under Air/H_2 gradient at 600–650 °C. The I–V and I–P curves (Fig. 3a) of a single cell show that the open-circuit voltages (OCV) of 0.97 V and 0.94 V were obtained at 600 °C and 650 °C, respectively, which are comparable values comparing with those measured for the furnace-sintered PCFC single cells [13] but are still 0.10–0.15V lower than the theoretical values. The sealing leakage was
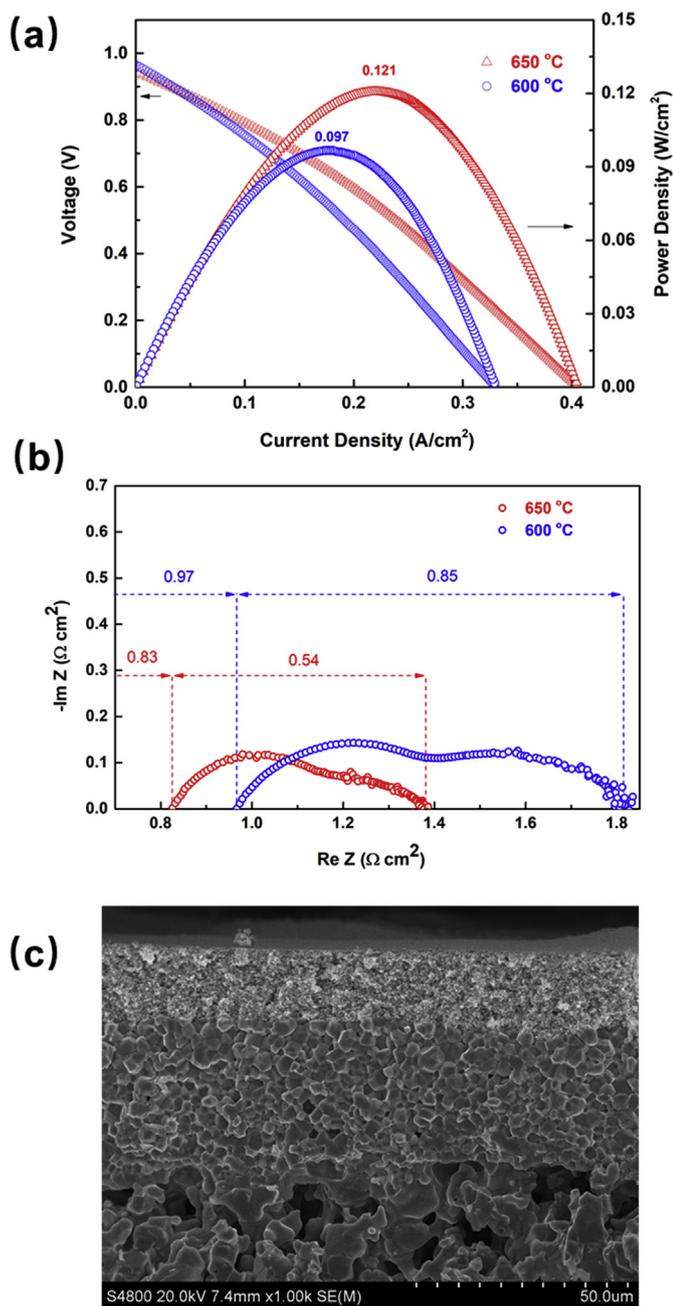
Fig. 3. Characterization of BCFZY0.1| RLRS-BCZYYb |Ni-BCZYYb single cell. (a) I–V and I–P curves, (b) electrochemical impedance spectra, and (c) SEM micrograph of the cell cross-section.

thought to be the main reason for the lower OCV because the separation of the sealant from electrolyte was observed after testing, while the microstructure of the single cells was kept well after testing. The peak power densities of the RLRS-derived single cell are 97 mW/cm^2 at 600 °C and 121 mW/cm^2 at 650 °C, which are not as high as the peak power density obtained for the state-of-the-art PCFC single cells fabricated by SSRS method [13]. The reason for the relatively low power density of the RLRS-derived single cell was analyzed by the electrochemical impedance spectroscopy (EIS). The EIS spectra of the RLRS-derived single cell at 600 °C and 650 °C are shown in Fig. 3b. The ohmic resistance (R_o) and polarization resistance (R_p) were substracted as follows: $R_o = 0.97 \, \Omega \, cm^2$ and $R_p = 0.85 \, \Omega \, cm^2$ at 600 °C, and $R_o = 0.83 \, \Omega \, cm^2$ and $R_p = 0.54 \, \Omega \, cm^2$ at 650 °C. Both the electrolyte resistance and the electrode resistance are relatively high. However, the SEM image (Fig. 3b) of this single cell after

testing indicates that the electrolyte thin film has a thickness of ~36 μm, which resulted in a proton conductivity of 3.7×10^{-3} S/cm for the RLRS-derived BCZYYb electrolyte, which is a moderate proton conductivity values comparing the BCZYYb electrolytes obtained by conventional methods. Therefore, the decreasing thickness of the electrolyte can result in high single-cell performance. Therefore, we can conclude that the PCFC single cells prepared by the RLRS method still have significant space to be further improved, and the RLRS is a promising fabrication method to allow independently adjust the electrolyte, anode, and cathode for achieving better PCFC performance. The rapid densification of protonic ceramic electrolyte and excellent bonding between electrolyte and electrode also can contribute to the rapid manufacturing of protonic ceramic energy devices using the newly developed integrated additive manufacturing and laser processing technique. Furthermore, the microstructure of tested BCZYYb electrolyte did not show obvious difference from the fresh BCZYYb just after the RLRS, which indicates that the RLRS has a good microstructure stability.

4. Conclusions

The state-of-the-art protonic ceramic electrolyte BaCe$_{0.7}$Zr$_{0.1}$Y$_{0.1}$Yb$_{0.1}$O$_{3-\delta}$ (BCZYYb) dense films were successfully deposited on as-prepared Ni(O)+BCZYYb anode substrate by recently developed rapid laser reactive sintering method. The separation of the preparation of dense electrolyte and porous anode makes it possible to manufacture protonic ceramic fuel cells (PCFCs) with more desirable electrolyte and anode microstructures. The PCFC single cells prepared after introducing the cathode thin film BaCo$_{0.4}$Fe$_{0.4}$Zr$_{0.1}$Y$_{0.1}$O$_{3-\delta}$ (BCFZY0.1) showed OCVs of 0.94–0.97V and peak power densities of 97 mW/cm^2 at 600 °C and 121 mW/cm^2 at 600–650 °C under Air/H$_2$ gradient. The proton conductivity of the BCZYYb film prepared by the RLRS technique showed a moderate proton conductivity of 3.7×10^{-3} S/cm at 600 °C. The higher PCFC performance can be expected by decreasing electrolyte film thickness and optimizing electrode microstructure.

Disclaimer

Declaration of competing interest

The authors whose names are listed immediately below certify that they have NO affiliations with or involvement in any organization or entity with any financial interest (such as honoraria; educational grants; participation in speakers' bureaus; membership, employment, consultancies, stock ownership, or other equity interest; and expert testimony or patent-licensing arrangements), or non-financial interest (such as personal or professional relationships, affiliations, knowledge or beliefs) in the subject matter or materials discussed in this manuscript.

Acknowledgments

the Fuel Cell Technologies Office Award Number DE-EE0008428.

Appendix A. Supplementary data

Supplementary data to this article can be found online at https ://doi.org/10.1016/j.powera.2020.100017.

References

[1] K.D. Kreuer, Proton-Conducting oxides, Annu. Rev. Mater. Res. 33 (2003) 333–359, https://doi.org/10.1146/annurev.matsci.33.022802.091825.

[2] C. Duan, D. Hook, Y. Chen, J. Tong, R. O'Hayre, Zr and Y co-doped perovskite as a stable, high performance cathode for solid oxide fuel cells operating below 500 °C, Energy Environ. Sci. 10 (2017) 176–182, https://doi.org/10.1039/C6EE01915C.

[3] C. Duan, R. Kee, H. Zhu, N. Sullivan, L. Zhu, L. Bian, D. Jennings, R. O'Hayre, Highly efficient reversible protonic ceramic electrochemical cells for power generation and fuel production, Nat. Energy 4 (2019) 230–240, https://doi.org/10.1038/s41560-019-0333-2.

[4] W. Wu, H. Ding, Y. Zhang, Y. Ding, P. Katiyar, P.K. Majumdar, T. He, D. Ding, 3D self-architectured steam electrode enabled efficient and durable hydrogen production in a proton-conducting solid oxide electrolysis cell at temperatures lower than 600 °C, Adv. Sci. 5 (2018) 1–9, https://doi.org/10.1002/advs.201800360.

[5] X. Li, M. Liu, S.Y. Lai, D. Ding, M. Gong, J.P. Lee, K.S. Blinn, Y. Bu, Z. Wang, L.A. Bottomley, F.M. Alamgir, M. Liu, In situ probing of the mechanisms of coking resistance on catalyst-modified anodes for solid oxide fuel cells, Chem. Mater. 27 (2015) 822–828, https://doi.org/10.1021/cm503852v.

[6] H. Ding, W. Wu, C. Jiang, Y. Ding, W. Bian, B. Hu, P. Singh, C.J. Orme, L. Wang, Y. Zhang, D. Ding, Self-sustainable protonic ceramic electrochemical cells using a triple conducting electrode for hydrogen and power production, Nat. Commun. 11 (2020), https://doi.org/10.1038/s41467-020-15677-z.

[7] H. Ding, W. Wu, D. Ding, Advancement of proton-conducting solid oxide fuel cells and solid oxide electrolysis cells at Idaho national laboratory (INL), ECS Trans. 91 (2019) 1029–1034, https://doi.org/10.1149/09101.1029ecst.

[8] W.G. Coors, A. Manerbino, Characterization of composite cermet with 68wt.% NiO and BaCe0.2Zr0.6Y0.2O3-δ, J. Membr. Sci. 376 (2011) 50–55, https://doi.org/10.1016/j.memsci.2011.03.062.

[9] Z. Zhao, J. Cui, M. Zou, S. Mu, H. Huang, Y. Meng, K. He, K.S. Brinkman, J. (Joshua) Tong, Novel twin-perovskite nanocomposite of Ba–Ce–Fe–Co–O as a promising triple conducting cathode material for protonic ceramic fuel cells, J. Power Sources 450 (2020) 227609, https://doi.org/10.1016/j.jpowsour.2019.227609.

[10] P. Babilo, T. Uda, S.M. Haile, Processing of yttrium-doped barium zirconate for high proton conductivity, J. Mater. Res. 22 (2007) 1322–1330, https://doi.org/10.1557/jmr.2007.0163.

[11] J. Will, A. Mitterdorfer, C. Kleinlogel, D. Perednis, L.J. Gauckler, Fabrication of thin electrolytes for second-generation solid oxide fuel cells, Solid State Ionics 131 (2000) 79–96, https://doi.org/10.1016/S0167-2738(00)00624-X.

[12] S. Choi, T.C. Davenport, S.M. Haile, Protonic ceramic electrochemical cells for hydrogen production and electricity generation: exceptional reversibility, stability, and demonstrated faradaic efficiency, Energy Environ. Sci. 12 (2019) 206–215, https://doi.org/10.1039/c8ee02865f.

[13] C. Duan, J. Tong, M. Shang, S. Nikodemski, M. Sanders, S. Ricote, A. Almansoori, R. OHayre, Readily processed protonic ceramic fuel cells with high performance at low temperatures, Science 349 (80) (2015) 1321–1326, https://doi.org/10.1126/science.aab3987.

[14] Q.L. Liu, K.A. Khor, S.H. Chan, X.J. Chen, Anode-supported solid oxide fuel cell with yttria-stabilized zirconia/gadolinia-doped ceria bilayer electrolyte prepared by wet ceramic co-sintering process, J. Power Sources 162 (2006) 1036–1042.

[15] C. Zhao, R. Liu, S. Wang, Z. Wang, J. Qian, T. Wen, Fabrication and characterization of a cathode-supported tubular solid oxide fuel cell, J. Power Sources 192 (2009) 552–555.

[16] S. Hossain, A.M. Abdalla, N. Radenahmad, A.K.M. Zakaria, J.H. Zaini, S.M.H. Rahman, S.G. Eriksson, J.T.S. Irvine, A.K. Azad, Highly dense and chemically stable proton conducting electrolyte sintered at 1200 °C, Int. J. Hydrogen Energy 43 (2018) 894–907, https://doi.org/10.1016/j.ijhydene.2017.11.111.

[17] S. Tao, J.T.S. Irvine, A stable, easily sintered proton-conducting oxide electrolyte for moderate-temperature fuel cells and electrolyzers, Adv. Mater. 18 (2006) 1581–1584, https://doi.org/10.1002/adma.200502098.

[18] S. Yang, S. Zhang, C. Sun, X. Ye, Z. Wen, Lattice incorporation of Cu 2+ into the BaCe 0.7 Zr 0.1 Y 0.1 Yb 0.1 O 3âî electrolyte on boosting its sintering and proton-conducting abilities for reversible solid oxide cells, ACS Appl. Mater. Interfaces 10 (2018) 42387–42396, https://doi.org/10.1021/acsami.8b15402.

[19] X. Xu, L. Bi, X.S. Zhao, Highly-conductive proton-conducting electrolyte membranes with a low sintering temperature for solid oxide fuel cells, J. Membr. Sci. 558 (2018) 17–25, https://doi.org/10.1016/j.memsci.2018.04.037.

[20] J. Tong, D. Clark, L. Bernau, M. Sanders, R. O'Hayre, Solid-state reactive sintering mechanism for large-grained yttrium-doped barium zirconate proton conducting ceramics, J. Mater. Chem. 20 (2010) 6333, https://doi.org/10.1039/c0jm00381f.

[21] S. Nikodemski, J. Tong, R. O'Hayre, Solid-state reactive sintering mechanism for proton conducting ceramics, Solid State Ionics 253 (2013) 201–210, https://doi.org/10.1016/j.ssi.2013.09.025.

[22] S. Nikodemski, J. Tong, C. Duan, R. O'Hayre, Ionic transport modification in proton conducting BaCe0.6Zr0.3Y0.1O3−δ with transition metal oxide dopants, Solid State Ionics 294 (2016) 37–42, https://doi.org/10.1016/j.ssi.2016.06.020.

[23] J.D. Morse, A.F. Jankowski, R.T. Graff, J.P. Hayes, Novel proton exchange membrane thin-film fuel cell for microscale energy conversion, J. Vac. Sci. Technol. A Vac., Surf., Film. 18 (2000) 2003–2005.

[24] X. He, B. Meng, Y. Sun, B. Liu, M. Li, Electron beam physical vapor deposition of YSZ electrolyte coatings for SOFCs, Appl. Surf. Sci. 254 (2008) 7159–7164.

[25] G. Meng, H. Song, Q. Dong, D. Peng, Application of novel aerosol-assisted chemical vapor deposition techniques for SOFC thin films, Solid State Ionics 175 (2004) 29–34.

[26] A.M. Kannan, P. Kanagala, V. Veedu, Development of carbon nanotubes based gas diffusion layers by in situ chemical vapor deposition process for proton exchange membrane fuel cells, J. Power Sources 192 (2009) 297–303.

[27] Y. Hong, J. Lei, M. Heim, Y. Song, L. Yuan, S. Mu, R.K. Bordia, H. Xiao, J. Tong, F. Peng, Fabricating ceramics with embedded microchannels using an integrated additive manufacturing and laser machining method, J. Am. Ceram. Soc. (2018) 1–12, https://doi.org/10.1111/jace.15982.

[28] S. Mu, Z. Zhao, J. Lei, Y. Hong, T. Hong, D. Jiang, Y. Song, W. Jackson, K.S. Brinkman, F. Peng, H. Xiao, J. Tong, Engineering of microstructures of protonic ceramics by a novel rapid laser reactive sintering for ceramic energy conversion devices, Solid State Ionics 320 (2018) 369–377, https://doi.org/10.1016/j.ssi.2018.03.023.

[29] H. Xiao, J. Tong, F. Peng, K. S. Brinkman, S. Mu, J. Lei, Y. Hong, H. Huang, R. Borida, Integrated additive manufacturing and laser processing systems and methods for ceramic, Glass Silicon Carbide Appl., 62/955,780.

[30] S. Mu, H. Huang, A. Ishii, Y. Hong, A. Santomauro, Z. Zhao, M. Zou, F. Peng, K.S. Brinkman, H. Xiao, J. Tong, Rapid laser reactive sintering for sustainable and clean preparation of protonic ceramics. https://doi.org/10.1021/acsomega.0c00879, 2020.

[31] S. Mu, Y. Hong, H. Huang, A. Ishii, J. Lei, Y. Song, A Novel Laser 3D Printing Method for the Advanced Manufacturing of Protonic Ceramics, 2020, pp. 1–17, https://doi.org/10.3390/membranes10050098.

[32] C. Wang, W. Ping, Q. Bai, H. Cui, R. Hensleigh, R. Wang, A.H. Brozena, Z. Xu, J. Dai, Y. Pei, C. Zheng, G. Pastel, J. Gao, X. Wang, H. Wang, J. Zhao, B. Yang, J. Luo, Y. Mo, B. Dunn, L. Hu, A general method to synthesize and sinter bulk ceramics in seconds 526 (2020) 521–526.

[33] F.W. Nyongesa, N. Rahbar, S.K. Obwoya, J. Zimba, B.O. Aduda, W.O. Soboyejo, An investigation of thermal shock in porous clay ceramics, ISRN Mech. Eng. 2011 (2011) 1–9, https://doi.org/10.5402/2011/816853.

[34] J. Yang, J. Yu, Y. Huang, Recent developments in gelcasting of ceramics, J. Eur. Ceram. Soc. 31 (2011) 2569–2591.

[35] P.M. Fan, K.F. Zhen, Z.Y. Zan, Z. Chao, Z. Jian, J.Z. Yun, Preparation and development of porous ceramic membrane supports fabricated by extrusion technique, Chem. Eng. Trans. 55 (2016) 277–282.

[36] M. Suzuki, M.S. Meddah, R. Sato, Use of porous ceramic waste aggregates for internal curing of high-performance concrete, Cement Concr. Res. 39 (2009) 373–381.

[37] P.N. Mollema, M.A. Antonellini, Compaction bands: a structural analog for anti-mode i cracks in aeolian sandstone, Tectonophysics 267 (1996) 209–228, https://doi.org/10.1016/S0040-1951(96)00098-4.

[38] S.H. Kim, S.R. Choi, D. Kim, Thermal Conductivity of Metal-Oxide Nanofluids: Particle Size Dependence and Effect of Laser Irradiation, 2007.

[39] V.V. Calmidi, R.L. Mahajan, The effective thermal conductivity of high porosity fibrous metal foams, J. Heat Tran. 121 (1999).

[40] G.R. Hadley, Thermal conductivity of packed metal powders, Int. J. Heat Mass Tran. 29 (1986) 909–920, https://doi.org/10.1016/0017-9310(86)90186-9.